JOC The Journal of Organic Chemistry

Article

Bringing a Molecular Plus One: Synergistic Binding Creates Guest-Mediated Three Component Complexes

S. Maryamdokht Taimoory, Kwaku Twum, Mohadeseh Dashti, FangFang Pan, Manu Lahtinen, Kari Rissanen, Rakesh Puttreddy, John F. Trant, and Ngong Kodiah Beyeh

J. Org. Chem., **Just Accepted Manuscript** • DOI: 10.1021/acs.joc.0c00220 • Publication Date (Web): 15 Mar 2020

Just Accepted

is published by the American Chemical Society. 1155 Sixteenth Street N.W., Washington, DC 20036

Bringing a Molecular Plus One: Synergistic Binding Creates Guest- Mediated Three Component Complexes

S. Maryamdokht Taimoory[†], Kwaku Twum[‡], Mohadeseh Dashti[†], Fangfang Pan[§], Manu Lahtinen[∥], Kari Rissanen*[∥], Rakesh Puttreddy*[∥‡], John F. Trant*[†], Ngong Kodiah Beyeh*[‡]

[†]University of Windsor, Department of Chemistry and Biochemistry, Windsor, ON, N9B 3P4, Canada

[‡]Oakland University, Department of Chemistry, 146 Library Drive, Rochester, MI 48309-4479, USA

[§]College of Chemistry, Key Laboratory of Pesticide & Chemical Biology of Ministry of Education, Central China Normal University, Luoyu Road 152, Wuhan, Hubei Province, 430079, People's Republic of China

[∥]University of Jyvaskyla, Department of Chemistry, P. O. Box 35, FI-40014, Jyväskylä, Finland

[‡]Tampere University, Faculty of Engineering and Natural Sciences, P. O. Box 541, FI-33101, Tampere, Finland

ABSTRACT: C_{Ethyl}-2-Methylresorcinarene (**A**), pyridine (**B**), and a set of ten carboxylic acids (**Cn**) associate to form **A·B·Cn** ternary assemblies with 1:1:1 stoichiometry, representing a useful class of ternary systems where the guest mediates complex formation between the host and a third component. Although individually weak in solution, the combined strength of the multiple non-covalent interactions organizes the complexes even in a highly hydrogen-bond competing methanol solution as explored by both experimental and computational methods. The interactions between **A·B** and **Cn** are dependent on the pKa values of carboxylic acids. The weak interactions between **A** and **C** further reinforce the interactions between **A** and **B**, demonstrating positive cooperativity. Our results reveal that the two-component system such as that formed by **A** and **B** can form the basis for the development of specific sensors for the molecular recognition of carboxylic acids.

INTRODUCTION

Cooperativity[1] among non-covalent interactions plays a crucial role in supramolecular chemistry.[2,3] When two components associate, each with multiple functional groups, the various non-covalent interactions will either reinforce or partially negate each other.[4] Advances in our understanding of these cooperative interactions has had a significant impact in diverse fields including pharmaceutical formulation,[5–9] energy,[10–14] and liquid crystalline materials.[15,16] These cooperative effects are further complicated in ternary systems and can include hydrogen[17] and halogen-bonded networks.[18,19] Complex multicomponent co-crystals have been primarily characterized by X-ray diffraction analysis,[20,21] however this provides less information about the solution-phase behaviour of these materials which is often of greater interest. Defined ternary complex formation is the result of the interplay between a number of factors that determine the overall thermodynamics, and structure: pKa value of acidic protons, electronic effects, electrostatics, polarization, resonance-assistance, and dipole-dipole interactions.[22] Making ternary complexes requires control of the non-covalent interactions in solution, particularly in protic polar solvents where hydrogen bonding is ubiquitous.[23] Control is rendered even more complicated as the co-operative binding interactions involved, although derived from the nature of the individual components, are true emergent properties of the complex itself.

Calixarenes, resorcinarenes, macrocyclic cavitands extensively studied for host-guest applications,[23–26] are well known for their ability to bind molecular guests *via* non-covalent interactions within their shallow and well-defined bowl-shaped cavity.[27] Two-component dimeric and hexameric capsules are common[28–30] but three-component all-organic structures involving macrocycles remain rare, and mostly involve either the host supported on a polymer or surface or polymer-like backbone,[31–34] or the host forming an inclusion complex with two guests simultaneously.[35–39] But research into these systems has overlooked a potentially useful topology.[3,40–43] Resorcinarenes have been proposed as useful point-of-care fluorescent diagnostics: for example, guest encapsulation changes the emission spectrum and can be used to measure binding.[44] However, a major limitation of

this application is that the choice of guest is restricted: small molecule heterocycles and salts are preferred. The utility of the systems would be greatly expanded by taking advantage of the emergent changes in the electronics of a bound guest to bind a third component, an analyte. This type of synergistic three-component interaction is typical for protein-ligand-protein, and protein-ligand-ligand in biological systems,[45] such as in the human leukocyte antigen system responsible for initiating immune responses,[46–48] but appears absent from the synthetic supramolecular receptor literature. Can a synthetic analogue of this system be envisioned? In a simple multi-component system, for example, binding a pyridine in the electron rich resorcinarene cavity should increase electron density on the nitrogen, potentially making it more basic; this could be exploited to bind a carboxylic acid, creating a guest-mediated ternary complex. This binding event would then further change the physical properties of the complex which could be observed. To the best of our knowledge this would be a new architecture for supramolecular constructs. However, resorcinarene-guest constructs often dimerize to form stable self-inclusion complexes: this needs to be less favourable than forming a three-component system: is it possible to keep the guest inside the host cavity, stabilized through multivalent interactions, when a ternary-component is added while preventing self-inclusion or capsule formation? Will binding of the third component be synergistic, as it is essential parameter for the co-crystal construction? Could this binding event be detected and justified using a joint experimental-*in silico* operation? These questions inspired the current study on a simple model system.

RESULTS AND DISCUSSION

Combining C_{ethyl}-2-methylresorcinarene (**A**) with pyridine (**B**) makes a simple, and well-defined 1:1 dimeric *endo*-complex (Scheme 1, Figure 1).[49–52] This was then titrated with ten different carboxylic acids (**Cn**; **n** = **1**-**10**) which should initiate a single strong $_{\mathbf{B}}$(N)···(H–O)$_{\mathbf{Cn}}$ interaction between **B** and **Cn**. Whether the ternary complex exists as hydrogen bonds and/or ion pairs[53-55] depends on the specific pKa values of **Cn** (Figure 1). Alternatively, by first mixing the **B** and **Cn**, we can make a strong hydrogen bond or ion-pair. The electron deficient pyridine that would be a better guest for **A**. We examined the monomeric, binary, and ternary components and complexes using NMR and isothermal titration calorimetry (ITC) to quantify the thermodynamics.

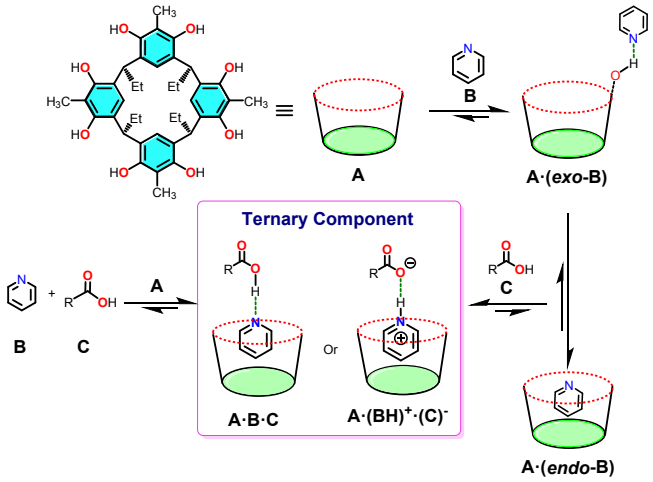

Scheme 1. Schematic representation of the stepwise assembly of ternary systems.

1. Solution Studies

1.1. NMR Analysis

Difluoroacetic acid exemplifies this analysis (**C2,** Figure 2). Only one set of signals is present in NMR spectra of the mixtures, indicating that the complexes are likely in fast dynamic equilibrium with the individual components. Mixing the acid (**C2**) and pyridine (**B**) together induces the expected deshielding of the aromatic proton resonances due to a decrease in aromatic electron density (Figure 2c *vs* 2b). Similarly, the **B** resonances become increasingly shielded when mixed with **A**, consistent with *endo*-complexation[30] (Figure 2d *vs* 2b). The H_d difluoroacetic acid proton experiences H-F coupling (Figure 2g). Mixing **C2** with **A** increases the splitting of the H_d signal but does not induce any significant changes in the chemical shift. This suggests that a weak hydrogen bond interaction induces asymmetry in the fluorine atoms, but that the interaction with the phenol does not result in a deprotonation (Figure 2f *vs* 2g).

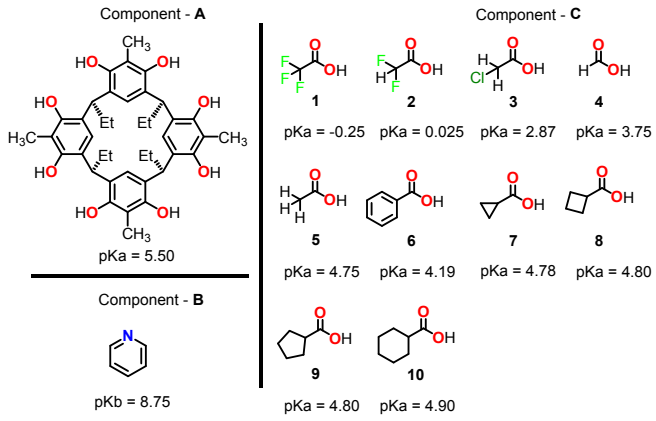

Figure 1. Components of the ternary complexes C_{ethyl}-2-methylresorcinarene (**A**), pyridine (**B**), and carboxylic acids (**Cn**).

The ^{1}H NMR spectra of ternary complex **A·B·C2** is clearly different from any of the binary systems it is derived from. In **A·C2**, the acid's H_d shows additional splitting but no significant shielding, suggesting that any interaction is *exo*. However, the change in the H_d chemical shift in the **A·B·C2** assembly is greater than that observed for **B·C2**, suggesting a greater degree of hydrogen bonding is occurring in **A·B·C2**: the nitrogen has become more basic. Similarly, the pyridine resonances are shielded, indicating stronger *endo*-cavity interaction with **A** than in the binary system alone.[56] This is significant as protonation of **B** in **B·C2** deshields the resonances; increased shielding in the ternary complex (Figure 2e) over **A·B**, means that increasing the host-guest interaction has a stronger impact on the chemical environment than the decrease in electron density arising from pyridinium formation.

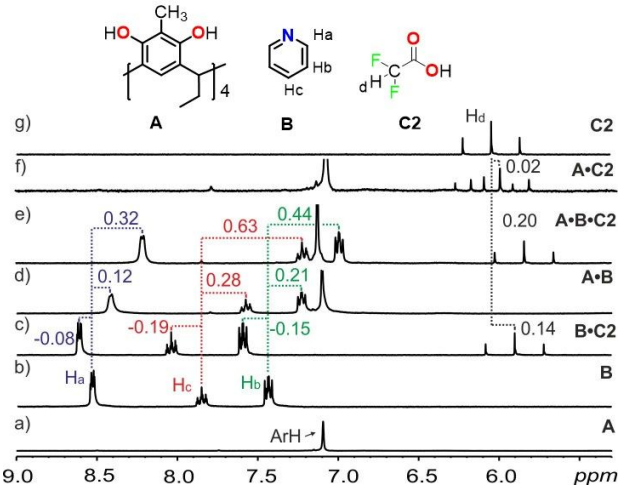

Figure 2. Expansions of the ^{1}H NMR (CD_3OD, 20 mM, 298 K, 300 MHz) of the three-component **A·B·C2** assembly of host **A**, the pyridine guest **B** and difluoroacetic acid, **C2** (pKa 0.025) and their dimeric and ternary complexes.

The same NMR experiments were conducted for the other **A·B·Cn** complexes. The degree of deshielding induced on **B** by the formation of **B·Cn** was proportional to the pKa of **Cn** (Figure 3). Clear deshielding of the pyridine resonances was observed with strong acids trifluoroacetic acid **C1**, difluoroacetic acid **C2**, chloroacetic acid **C3**, and formic acid **C4** (Figure S1-S4). Negligible changes were seen with the weaker acids **C5**-**C10** (Figures S5-S10). Similarly, the increase in shielding of the **B** protons in **A·B·Cn** compared to **A·B** also increased as a function of pKa for **C1**-**C4**. For the weaker acids **C5**-**C10**, no significant increase in **B** shielding was observed between **A·B** and **A·B·Cn** suggesting that the pyridine's position and interactions within the host cavity is not hugely affected by binding to the weaker acids. For the reported ternary systems, we made an approximation that **A·B** are in equilibrium and treated as one entity. **Cn** were titrated into an equimolar mixture of **A** and **B**. With this approximation, when **C** is added, the equation for the binary process was employed.[57] Due to this approximation, the experimental binding constants for the ternary system are relative, and the absolute value must be carefully interpreted and mainly provides for ready comparison with the computational analysis (Table 3).

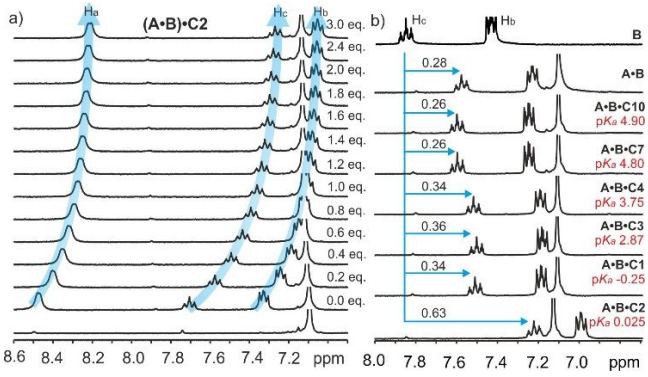

Figure 3. Expansions of the ^{1}H NMR spectra (CD_3OD, 20 mM, 298 K, 300 MHz) of (a) the titration of acid **C2** into an equimolar mixture of **A** and **B**; and (b) the ternary complexes. Shift changes of the resonances, labels are in ppm.

To further support these observations, ^{19}F NMR studies were carried out on **A·B·C2** as fluorine's chemical shift is very sensitive to the chemical environment. The -CF_2H signal was shielded by 0.24 ppm in the equimolar mixture of **A** and **C2** indicating some interaction between the components (Figure 4b). A significant deshielding of -1.85 ppm was observed for **B·C2**, indicating a strong $_{\mathbf{B}}$(N)···(H–O)$_{\mathbf{C2}}$ hydrogen bond interaction (Figure 4c), while in **A·B·C2**, an even more significant deshielding (–2.60 ppm) of the fluorine signal was observed suggesting cooperativity (Figure 4d). A similar phenomenon but with much smaller shift changes of the fluorine signals was observed with the trifluoroacetic acid **C1** in **A·B·C1** (Figure S2).

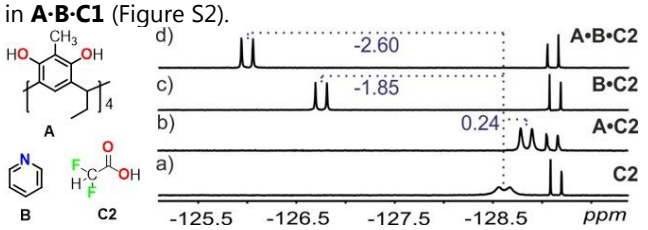

Figure 4. Sections of the ^{19}F NMR (CD_3OD, 298 K, 300 MHz) of the three-component ternary **A·B·C2** assembly between the host **A**, the pyridine guest **B** and difluoroacetic acid, **C2** (pKa 0.025). Spectra are produced from (a) **C2**. Equimolar mixture of: (b) **A** and **C2**, (c) **B** and **C2**, (d) **A**, **B**, and **C2**. Dashed lines highlight the observed shift changes of the resonances, labels are in ppm.

1.2. DOSY NMR Analysis

DOSY further supports the presence of these ternary complexes. The diffusion coefficient of a molecular species depends on its molecular weight, solvodynamic radius, and interactions with solvent.[58–60] When comparing similar species in the same solvent at the same concentration and the same temperature, a smaller diffusion coefficient indicates a larger species. We studied a strong (**C2**) and a

weak (**C10**) acid with monitorable protons (trifluoracetic acid **C1** is not suitable due to the lack of a C–H bond). The diffusion coefficient of **A** (20 mM) in CD_3OD at 298 K was 0.63×10^{-9} m^2s^{-1} (Table 1, Figure 5),[61] consistent with other previously reported resorcinarene-derived values confirming that no dimeric or hexameric capsule is present.[59,60] The diffusion coefficients for the **B** and the acids (**C2** and **C10**) also reflect their different solvodynamic radii in methanol (Table 1). When dimer and ternary structures are formed, the diffusion coefficients decrease, indicating slower movement, and likely a larger hydrodynamic radius. Taking the 1:1 host-guest mixture of **A** and **B** as an example, the diffusion coefficients of host **A**, and **B** dropped to 0.59×10^{-9} m^2s^{-1} and 1.91×10^{-9} m^2s^{-1} respectively. In a capsular construct, the diffusion coefficients would be the same. However, as an open inclusion complex it is in dynamic equilibrium with the monomeric species, and these different diffusion coefficients are expected. In the 1:1 mixture of **B** and **C2**, the decrease in the diffusion coefficients of both **B** and **C2** show they both participate in a larger assembly; however, in the **C10** and **B** complex, the diffusion coefficients resemble those of the free species consistent with a much weaker interaction (Table 1, Figure S30).

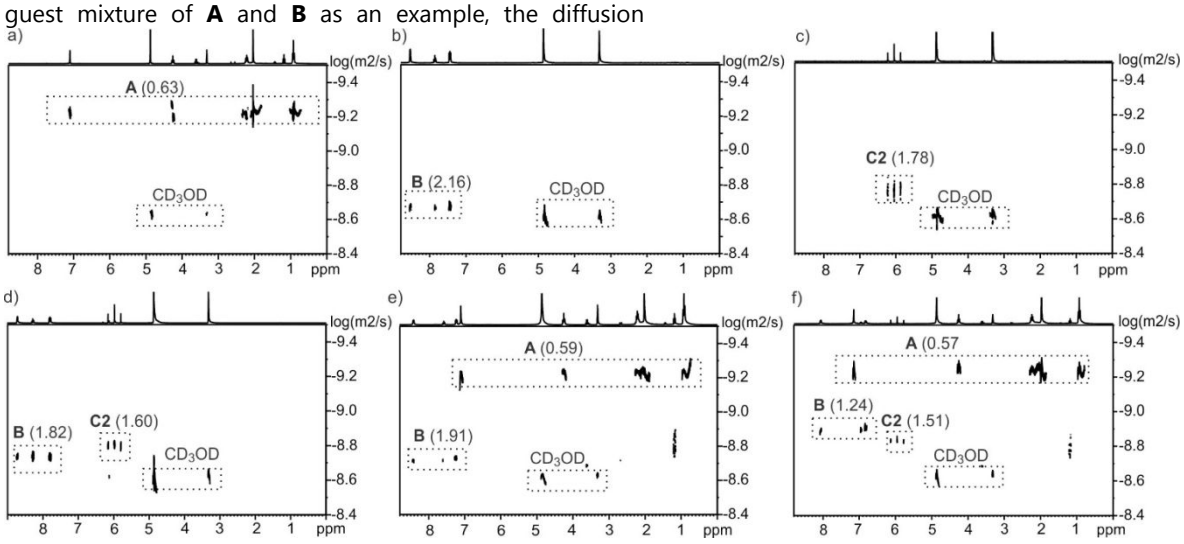

Figure 5. 2D DOSY NMR spectra (in CD_3OD at 298 K) of a 20 mM sample of: a) **A**, b) **B**, c) **C2**, and equimolar mixtures of d) **B**+**C2**, e) **A**+**B**, f) **A**+**B**+**C2** showing the chemical species present in the samples. The diffusion coefficient ($\times10^{-9}$ m^2s^{-1}) of each species is shown in brackets.

Considering the host-acid dimers (**A·C2** and **A·C10**), we see that the interaction is weak: addition of the acid has little to no effect on the diffusion coefficient of the host (Table 1, Figure S31). Considering **A·B·C2** the diffusion coefficients of all components drop precipitously from all binary species: the size difference would not be significant (as can be seen by the minor change in **A**). This decrease in the values of **B** and **C** are consistent with the equilibrium now lying more towards the complex (Table 1, Figure 5, and Figure S31). In the case of the **C10** ternary complex, the changes are far more subtle. The diffusion coefficients for **C10** and **B** are lower than in their dimeric pair, but the decrease is not as significant, again consistent with the ^{1}H NMR data. The shifts are moderated as the process was measured in methanol, which competes for hydrogen bonds, decreasing affinity. In previous investigations of dynamic enclosed capsular resorcinarene-based assemblies, methanol was routinely used as a competing hydrogen bond solvent to actually break-up the capsular assemblies.[60] Seeing these effects in this solvent is strong evidence of the high affinity these components have for each other, especially in the presence of a competing solvent.

All of these results are supported by the NOESY analysis (Figures S32-33). In ternary complex **A·B·C2**, the pyridine and the host clearly show strong through space interactions that are only consistent with an *endo*-inclusion complex. The fluorine resonances on the acid show exchange peak behaviour with respect to the host phenolic protons. This indicates either rapid changes in conformation, or rapid exchange between bound and unbound forms. Together, all of the NMR evidence supports the formation of the proposed guest-mediated ternary system.

Table 1. Average diffusion coefficients D^a ($\times10^{-9}$ m^2s^{-1}) of the species in different combinations in CD_3OD^b at 298 K. The mixtures are all equimolar.

	A	**B**	**C2**	**C10**	CD_3OD
A	0.63	–	–	–	2.61
B	–	2.16	–	–	2.39
C2	–	–	1.78	–	2.47
C10	–	–	–	1.40	2.23
A+B	0.59	1.91	–	–	2.36
B+C2	–	1.82	1.60	–	2.35
B+C10	–	2.14	–	1.44	2.41

A+C2	0.58	–	1.80	–	2.38
A+C10	0.59	–	–	1.12	2.33
A+B+C2	0.57	1.24	1.51	–	2.32
A+B+C10	0.59	1.85	–	1.15	2.32

[a]Standard deviation < 5%. [b]Diffusion coefficient of CD_3OD is ~2.38×10^{-9} m^2s^{-1}.[62]

1.3. ITC Analysis

DOSY and ^1H NMR suggest the presence of a synergistic binding mode, but the gold-standard approach for measuring binding affinity is ITC, and for comparison the measurements were conducted in methanol (Figures S34-35). The thermodynamic parameters of host-guest binding (*K*, ΔH, ΔS, and ΔG) for the binary components were determined by fitting the ITC data to a one-site binding model (Table 2, See Table 3 for ^1H NMR derived association constants). Negative ΔG values reveal the binding to be spontaneous at 303 K. The negative ΔH and TΔS values for the **B·Cn** and **A·B·Cn** systems indicate the complexation to be enthalpy driven, but entropy compensated. The negative ΔH and positive TΔS value for **B·C10** indicates that the process is favored by both enthalpy and entropy (desolvation) driven. Resorcinarene **A** and pyridine **B** dimerize with a binding constant of 301 M^{-1}. The interaction between **B** and the carboxylic acids reveal a binding constant of 533 M^{-1} for strong acid **C2** and 70 M^{-1} for the weak acid **C10**. This means that at equilibrium, **A** and **B** essentially exist as the dimer, while **B** and **C2** also exist as the hydrogen-bonded ion pair, while in **B·C10** the interaction is far weaker. ITC is designed to determine the thermodynamics of two-component systems; there is no method to compute the thermodynamics of a system consisting of three independent components interacting simultaneously. However, in the case of **B·C2** we can assume that it behaves largely as a single component as the binding is strong. Titrating host **A** into an equimolar mixture of these compounds allowed the data to be fitted to a one-site binding model with a binding constant of 671 M^{-1}. The fact that this value is larger than the observed binding constant of **A·B** (301 M^{-1}) means that the-pyridinium cation is a better guest than the neutral pyridine. Binding between **B** and **C10** was insufficient for the required assumption that the mixture act like a single molecule: there is enough free **B** or **A·B** to prevent the mathematical model from providing a fit. This is not surprising; ITC is not designed to calculate three-component interactions, the fact that **B·C2** form a strong enough dimer that it can be treated as a discrete single species is exceptional—we could not find any examples in the literature where it had been used for this previously. However, the assumption is clearly fair for **C2** as the **B·C2** system acted as a single unit, a prerequisite for ITC parameter calculation. The solution phase studies all strongly indicate that proposed guest-mediated complexes are formed and that formation is synergistic with respect to all possible binary complexes.

Table 2. Binding constants *K* [M^{-1}] calculated for the **A·B**, **B·Cn** system and **A·B·Cn** ternary system

Entry	*K* [M^{-1}]	ΔH (kcal/mol)	TΔS (kcal/mol)	ΔG (kcal/mol)
A·B	301±80	-38.2±0.3	-34.9	-3.3
B·C2	533±46	-16.9±0.7	-13.2	-3.7
B·C10	70±1	-0.2±0.5	2.4	-2.6
A·(B·C2)	671±200	-7.7±0.8	-3.8	-3.9
A·(B·C10)	–[b]	–[b]	–[b]	–[b]

[a]ITC was done in CH_3OH at 298 K. [b]Data could not be fitted due to sufficient deviation from a two-component system.

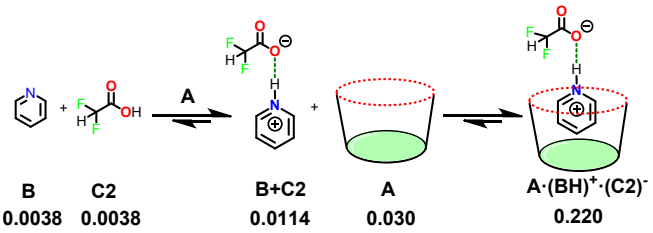

Scheme 2. Representation of the approximate equilibrium concentrations (M) of **A**, **B**, and **C** and their complexes at 0.25 M, illustrating the synergy of binding shown in Table 2.

2. X-Ray Crystallography

Crystallizing **A·Cn** binary complexes is highly challenging and, we only obtained a crystal of **A·C6** (Figure S46). Benzoic acid dimers, typically observed in solid-state X-ray crystal structures, do not generate a beneficial alignment for resorcinarene *endo*-complexation processes. Therefore, in the **A·C6** binary complex, the host cavities are stabilized by self-inclusion while the hydrogen bonded benzoic acid dimers simply occupy 3-D crystal lattice. Our repeated attempts to grow single crystals of **B·Cn** components from various solvents provided only pyridinium trifluoroacetate, **B·C1**, as a crystalline material (See Figure S45). To our surprise, no SCXRD reports on pyridinium co-crystals of the type, $(\mathbf{BH})^+\cdot\mathbf{Cn}^-$, except for co-crystal **B·C1**, could be found in the Cambridge Structural Database (CSD).[63] The X-ray crystal structure of **A·B** contains a resorcinarene self-inclusion complex where the pyridine (**B**) resides outside the host cavity (Figure S44). None of these structures are auspicious building blocks for the ternary complexes observed in solution. Fortunately, the ternary complexes behave differently: **A** reduces the molecular motion of **B** through C–H···π and π-π interactions and combined with the strong hydrogen bond/ion pair formed between the pyridine and **Cn** provides sufficient lattice energy to yield single crystals for X-ray diffraction analysis.

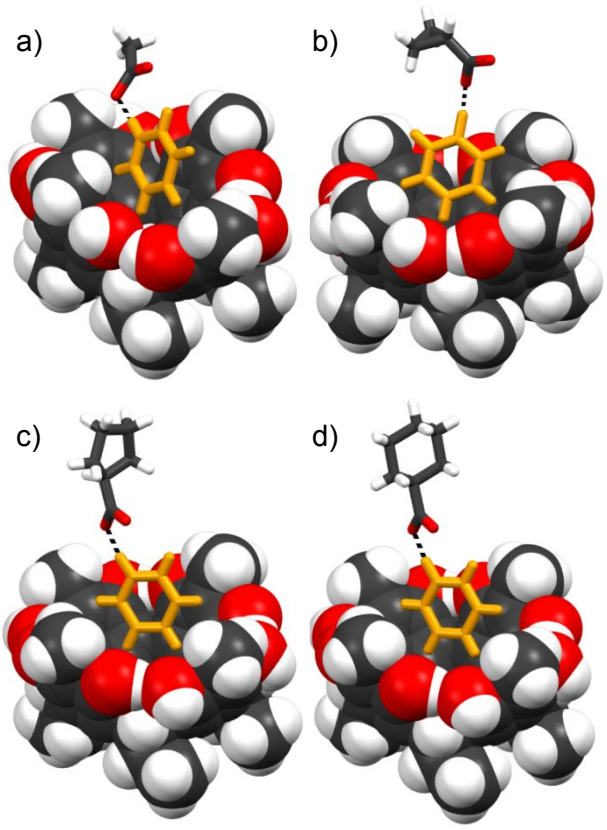

Figure 6. X-Ray crystal structure of ternary co-crystals a) **A·B·C5**, b) **A·B·C7**, c) **A·B·C9** and d) **A·B·C10**. Dashed black-lines highlight the hydrogen bonding, orange capped-stick model represents protonated **B** and disordered fragments are omitted for clarity.

Of the ten potential ternary systems, we obtained SCXRD data for five **A·B·Cn** ternary complexes (n = **1**, **5**, **7**, **9**, and **10**; Figures 6 and S47). All adopt the same core geometry: **B** resides, protonated, inside **A**'s cavity and interacting with the carboxylate through the $_{\mathbf{B}}(N–H)^{+}\cdots(^{-}O)_{\mathbf{Cn}}$ hydrogen bond. In **A·B·C5**, **B** sits deeper inside the host cavity at a position 2.51 Å from the centroid of the lower rim carbon atoms, compared to **A·B·C1** [3.04 Å], **A·B·C7** [2.74 Å], **A·B·C9** [2.94 Å], and **A·B·C10** [2.95 Å]. The shortest $_{\mathbf{B}}(C–H)\cdots(\pi)_{\mathbf{A}}$ contact was observed between pyridine H-atom and the *endo*-cavity host carbon in **A·B·C1** [2.41 Å]. The contact distances in the other systems vary: **A·B·C5** [2.50 Å], **A·B·C7** [2.67 Å], **A·B·C9** [2.52 Å], and **A·B·C10** [2.55 Å].

3. Computational Studies

We performed computational modelling on these multi-component assemblies to probe the structural and energetic aspects of this ternary assemblies applying ωB97X-D/6-311G** level of theory11, with the polarized continuum solvation model (PCM) to consider the solvent effects. As examples for discussion, the energies for the binary and ternary components, **A·C1**, **A·B**, **B·C1** and **A·B·C1** are shown in Figure 7 (see Supporting Information for all optimized structures). The thermodynamic parameters for ternary assemblies calculated in two different ways [1). $\Delta E = E_{\mathbf{A\cdot B\cdot C}} - E_{\mathbf{A}} - E_{\mathbf{B}} - E_{\mathbf{C}}$, and 2). $\Delta E = E_{\mathbf{(A\cdot B)\cdot C}} - E_{\mathbf{A\cdot B}} - E_{\mathbf{C}}$] shows the same energetic trends and highlighted in Table 3. In **A·C1**, the $_{\mathbf{A}}(O–H)\cdots(O–H)_{\mathbf{C1}}$ hydrogen bonds are moderately strong[64] (Figure 7a). In **B·C1**, the expected tight hydrogen bonded ion-pair $_{\mathbf{C1}}(O^{-})\cdots(H–N^{+})_{\mathbf{B}}$, similar to that observed in the X-ray crystal structure (Figure S37), is formed. In **A·B** despite the symmetry of the host, the *endo*-cavity pyridine ring does not face straight up. Instead it is oriented at an angle, allowing it to form $_{\mathbf{B}}(C–H)\cdots(\pi)_{\mathbf{A}}$ interactions with the host cavity using acid C–H protons *ortho*- and *para*- to the N-atom, in addition to the expected $\pi_{\mathbf{B}}$-$\pi_{\mathbf{A}}$ interactions (Figure 7c). The interactions in each binary component, discussed above, combine synergistically to define **A·B·C1**. The deprotonated **C1** oxygen further stabilizes this complex through $_{\mathbf{C1}}(C=O)\cdots(O–H)_{\mathbf{A}}$ hydrogen bonds (Figure 7d).

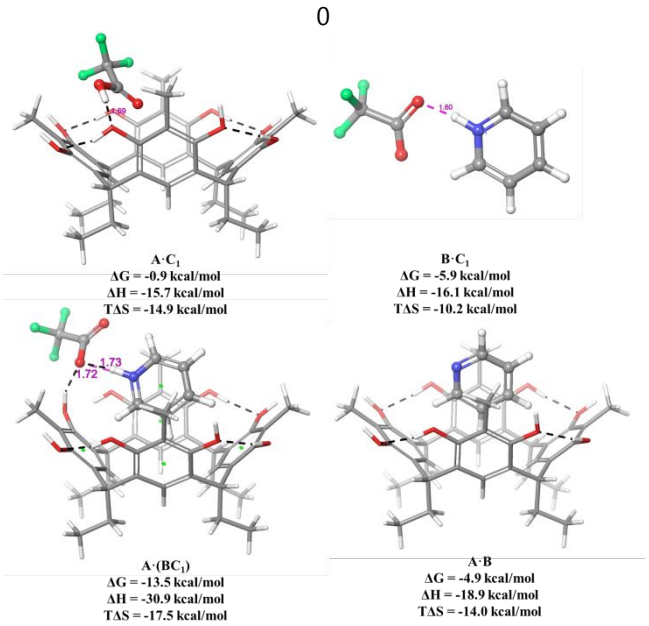

Figure 7. The computed thermodynamic parameters for binary components of **A·C1**, ($\Delta G = G_{\mathbf{A\cdot C1}} - G_{\mathbf{A}} - G_{\mathbf{C1}}$), **A·B**, ($\Delta G = G_{\mathbf{A\cdot B}} - G_{\mathbf{A}} - G_{\mathbf{B}}$), **B·C1**, ($\Delta G = G_{\mathbf{B\cdot C1}} - G_{\mathbf{B}} - G_{\mathbf{C1}}$), and ternary component **A·B·C1** ($\Delta G = G_{\mathbf{A.B.C1}} - G_{\mathbf{A}} - G_{\mathbf{BC1}}$).

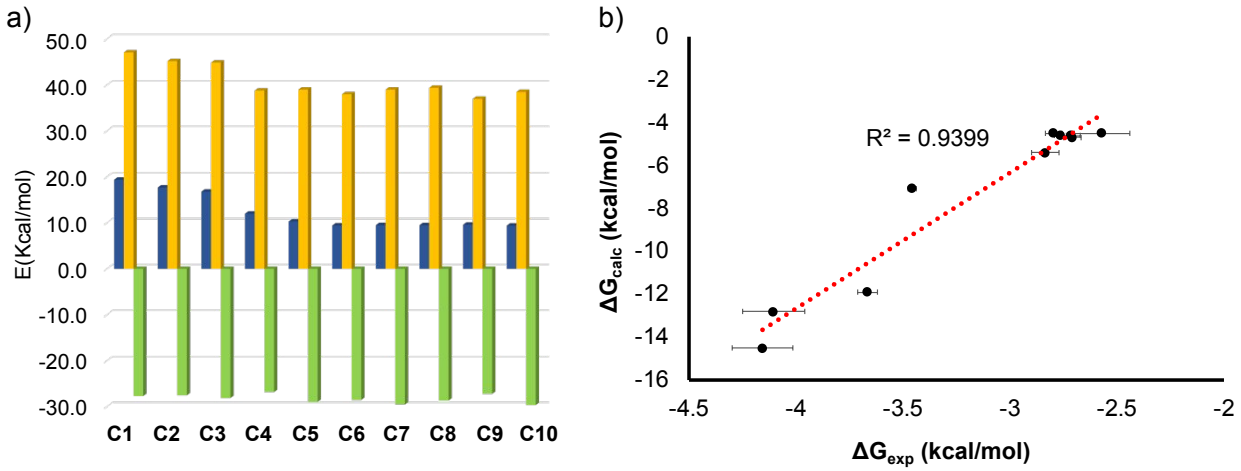

Figure 8. (a) The calculated binding free energy (ΔG times negative sign, (–) * (ΔG) blue), enthalpy (ΔH times negative sign, (–) * ΔH, yellow), and entropy (+TΔS, times negative sign, (–) * TΔS green) of (a) **A·B·Cn** in MeOH (PCM); (b) Linear correlation of the experimental free energy of binding ΔG_{exp} of the **A·B·Cn** ternary complexes with predicted binding free energies (ΔG_{calc}).

Table 3. The calculated thermodynamic parameters and key atomic distances of the ternary complexes **A·B·C** ($\Delta G = G_{A\cdot B\cdot C} - G_A - G_B - G_{C1}$); ($\Delta H = H_{A\cdot B\cdot C} - H_A - H_B - H_C$); $T(\Delta S = S_{A\cdot B\cdot C} - S_A - S_B - S_C)$. The values in the brackets are the calculated thermodynamic parameters for the association of **Cn** with the binary complex **A·B** (defined as $\Delta G = G_{(A\cdot B)\cdot C} - G_{A\cdot B} - G_C$; $\Delta H = H_{(A\cdot B)\cdot C} - H_{A\cdot B} - H_C$; $T(\Delta S = S_{(A\cdot B)\cdot C} - S_{A\cdot B} - S_C)$ which is comparable to the values obtained from the NMR data (ΔG_{Exp}).

Entry	$_B(N)\cdots(H–O)_{Cn}$	$_{Cn}(O–H)\cdots(O–H)_A$	ΔH_{calc} (kcal/mol)[a]	$T\Delta S_{calc}$ (kcal/mol)[a]	ΔG_{calc} (kcal/mol)[a]	K_{aExp}[b]	ΔG_{Exp} (kcal/mol)[a]
A·B·C1	1.05	1.72	-47.1 (-28.2)	–27.7 (–13.7)	–19.4 (–14.5)	1173 ± 40	–4.2 ± 0.2
A·B·C2	1.06	1.71	–45.2 (–26.4)	–27.5 (–13.5);	–17.7 (–12.8)	1073 ± 38	–4.1 ± 0.2
A·B·C3	1.06	1.69	–44.9 (–26.0)	–28.1 (–14.1)	–16.8 (–11.9)	509 ± 6	–3.7 ± 0.1
A·B·C4	1.07	1.64	–38.8 (–19.9)	–26.9 (–12.8)	–12.0 (–7.1)	357 ± 2	–3.5 ± 0.1
A·B·C5	1.07	1.60	–38.0 (–19.1)	–28.5 (–14.5)	–9.5 (–4.6)	116 ± 2	–2.8 ± 0.1
A·B·C6	1.58	1.77	–39.0 (–20.2)	–29.6 (–15.5)	–9.5 (–4.6)	110 ± 1	–2.8 ± 0.1
A·B·C7	1.08	1.61	–37.0 (–17.9)	–27.2 (–13.2)	–9.6 (–4.7)	100 ± 2	–2.7 ± 0.1
A·B·C8	1.08	1.61	–38.8 (–20.0)	–28.7 (–14.6)	–9.5 (–4.6)	101 ± 2	–2.7 ± 0.1
A·B·C9	1.07	1.59	–39.0 (–20.2)	–29.0 (–14.7)	–10.3 (–5.4)	124 ± 3	–2.8 ± 0.1
A·B·C10	1.07	1.59	–38.5(–19.6)	–29.6 (–15.1)	–9.4 (–4.5)	79 ± 4	–2.6 ± 0.1

[a]The calculated thermodynamics of ternary complexes estimated in three different mechanistic ways defined as a) **A·B·C** ($\Delta G = G_{A\cdot B\cdot C11} - G_A - G_B - G_C$); ($\Delta H = H_{A\cdot B\cdot C} - H_A - H_B - H_C$); $T(\Delta S = S_{A\cdot B\cdot C} - S_A - S_B - S_C)$; b) The calculated thermodynamic parameters for the association of **Cn** with the binary complex **A·B** defined as $\Delta G = G_{(A\cdot B)\cdot C} - G_{A\cdot B} - G_C$; $\Delta H = H_{(A\cdot B)\cdot C} - H_{A\cdot B} - H_C$; $T(\Delta S = S_{(A\cdot B)\cdot C} - S_{A\cdot B} - S_C)$reported in order. [b]The experimental data was acquired from the NMR titrations (Figure 1). The titrations provide an estimate of the binding constant, and the Gibbs' free energy can be calculated from this parameter. The experimental data treats a 1:1 equimolar solution of A and B as dimeric complex AB as a single unit introducing error into the measurement. For all proposed mechanistic scenarios see table S2.

Since **Cn** is the only component that differs between any two ternary systems, it would be unsurprising if the stability of the complexes is highly dependent on the pKa of the acid. This would be expected to be especially true if one is simply analyzing the interaction between the pyridine and the acid as a binary system. However, this is not the case. Due to the steric demands of the different acids, the pKa values of the carboxylic acids alone do not correlate or predict with the binding free energies of **B·Cn** dimers (R^2 = 0.5, Figure 9). Interestingly, a far better free energy correlation with the **Cn** acidic strength is obtained in **A·B·Cn** complexes with R^2 = 0.86 (Figure 9) compared with the predicted binding free

energies of **B·Cn** dimers. This result supports co-operativity: pKa is more important in the ternary system than in a simple binary acid-base system because the acidity and basicity behavior are enhanced. The presence of the resorcinarene, by increasing electron density on the pyridine and decreasing it on the acid, increases the affinity of the acid for the base.

Ternary assemblies involving the stronger acids **C1-C4** feature stronger intermolecular hydrogen bonding and/or hydrogen bond ion-pair interactions (as judged based on the distance contacts between N-atom of the *endo*-pyridine and carboxylic acid functional group) compared to their simple **B·Cn** binary complexes. The stronger acids either form stronger $_{Cn}(O–H)\cdots(N)_{B}$ or $_{Cn}(O^{-})\cdots(H–N^{+})_{B}$ hydrogen bond interactions improving the dispersion corrected binding energies ($E_{binding}$) calculated as A) the binding energy between host, **A**, and the **B·C** binary assembly in their ternary complex geometry $E_{(B\cdot C)\cdot A} - E_{B\cdot C} - E_{A}$ are larger ranging from –28.4 kcal/mol to –36.6 kcal/mol for **A·B·C1-4** complexes than **A·B·C5-10** ranging from –25.6 kcal/mol to –26.0 kcal/mol. In addition, to be consistent with NMR titration study of **A·B** treated as one entity and in equilibrium with **C**, the calculated binding energy of $E_{(A\cdot B)\cdot C} - E_{A\cdot B} - E_{C}$ are ranging from –31.1 to –40.4 kcal/mol for **A·B·C1-4** complexes and are ranging from –22.6 to –30.8 kcal/mol **A·B·C5-10**.
On the other hand, the $_{Cn}(O–H)\cdots(O–H)_{A}$ interactions between carboxylic acids and host hydroxyl group in **A·B·C1-4** are weaker compared to those in **A·B·C5-10** (Table 3). In **A·B·C5-10**, the hydrophobic aggregation between carboxylic acid bulky backbones and the host methyl groups also influences binding energies in calculated structures. In those structures, a balanced combination of steric interactions, weak hydrogen bonds, and electrostatic factors contributes to their decreased free energy and binding enthalpy (Figure S53; Table 3). When compared to the experimentally-determined binding energies, the computational calculations systematically overestimate the binding. This might partially arise from the assumptions around the solvation model of these systems, but could also arise from limitations to the experimentally-derived measurements which were determined using the ^{1}H NMR shifts. This systematic discrepancy is not atypical for these types of comparisons, and what is notable is that the trends observed experimentally are mirrored in the computational analyses (Figure 8b).

Evidence of cooperativity effects in the ternary assembly

The cooperativity derived differences in the thermodynamics of **A·B·C1-10** versus **A·B**, **B·C1-10**, and **A·C1-10** can be evaluated. The hydrogen bond interactions between **B** and **C** in **A·B·Cn** systems improves the **A·B** host-guest interactions within the cavity (positive cooperativity).[65–67] In addition to the obvious **B** and **Cn** interactions, the interactions between **A** and **Cn** also modulate the formation of the **A·B·Cn** complex, reinforcing the strength of the non-covalent interactions within the assembly binding **B** and **A** as well as **B** and **Cn** together.

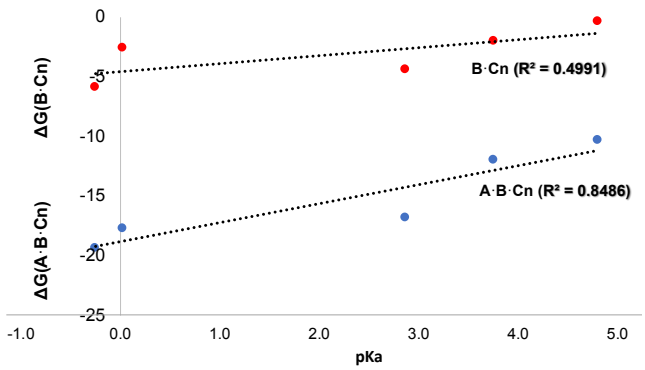

Figure 9. The calculated Gibbs free energy of ternary hydrogen-bonded complexes and binary complexes in MeOH (PCM) solvation model vs pKa values of carboxylic acid molecules.

The Williamson cooperativity model,[66,67] a thermodynamic data cyclic process that quantifies the cooperativity in multicomponent systems by using four equilibrium constants (K_n, n = 1-4) and their corresponding free energies (ΔG_n , n = 1-4), was applied to these **A·B·Cn** ternary systems. This proposed model provides further insights into the binding interactions between the **A**, **B**, and **Cn** components. As an example, the model for **A·B·C2** is shown in Figure 10 (for more examples, see Figure S54). According to this model, in the **A·B·C2** system, guest **B** binds to either **C2** or **A**, to give the respective binary components **B·C2** and **A·B**. The corresponding free energies are ΔG_1 = –2.6 kcal/mol (K_1, clockwise) and ΔG_2 = –4.9 kcal/mol (K_2, anti-clockwise), respectively.

Addition of **A** to **B·C2**, and **C2** to **A·B** generates free energies of ΔG_4 = –15.1 kcal/mol (K_3, clockwise) and ΔG_3 = –12.8 kcal/mol (K_4, anti-clockwise), respectively. In both the clockwise or anticlockwise route, the coupling free energy, $\Delta\Delta G = \Delta G_1 - \Delta G_4 = \Delta G_2 - \Delta G_3$, is defined as the free energy upon addition and removal of the same third component. In other words, G is the free energy generated by the formation or breaking of new binding interactions during addition or removal of the same third component, at two different reaction stages, within an **A·B·Cn** system. The coupling free energies of 10.1 kcal/mol and 10.2 kcal/mol for **A·B·C2** suggests that both routes are cooperative and thermodynamically favourable. In both routes the stronger interaction forms second in line reflecting the Williamson model suggesting the ternary complex formation is a synergistic process.

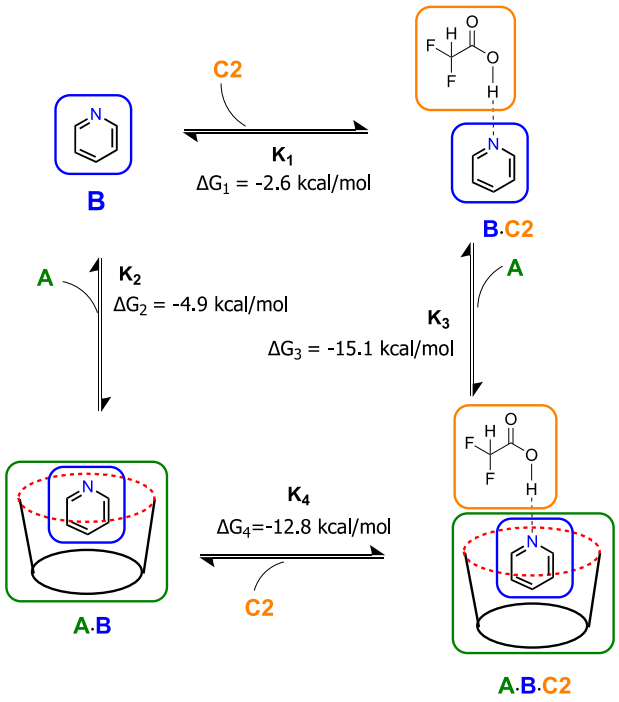

Figure 10. Williamson cooperativity model for **A·B·C2** showing the calculated energies of the binding interactions and that the two possible overall pathways both proceed through a first favourable binding interaction followed by a strongly favourable binding of the third component. The difference between ternary formation and binary formation can be taken as the calculated co-operative energy of the process.

CONCLUSIONS

The reported pyridine-mediation of a resorcinarene-carboxylic acid interaction represents a clear example of this ternary supramolecular archetype. The formation of these 1:1:1 stoichiometric systems are investigated both in solution and as solid-state co-crystals, and their strongly positive co-operative association is supported by *in silico* analysis. The presence of the carboxylic acid, located outside the cavity, stabilizes the pyridine-resorcinarene inclusion complex. The electron-rich resorcinarene cavity makes the pyridine N-atom more basic via the host-guest C–H···π interactions. In the ternary systems, the strength of the O–H···N hydrogen bond between *exo*-carboxylic acid and *endo*-pyridine varies from −104.0 kcal/mol to −121.0 kcal/mol for carboxylic acids with pKa values ranging between −0.25 and 3.75; and −37.0 kcal/mol to −102.0 kcal/mol for acids with pKas between 4.19 and 4.90. The ITC derived thermodynamic parameters, negative ΔH and positive TΔS values, for carboxylic acid-pyridine (binary) and ternary systems indicate that complexation is enthalpy driven and compensated by entropy. This was supported by *in silico* ternary experiments showing complexation is driven by favourable enthalpy that overcomes the entropic barrier. Furthermore, the DFT calculations support the positive cooperativity between three components according to a Williamson model. By broadening the pool of analytes for supramolecular diagnostic tools from those that fit in a macrocycle's cavity, to include those that interact with the guests in the cavity, these guest-mediated ternary complexes could prove very useful as the basis for next-generation sensors in biomedicine and environmental science applications.

EXPERIMENTAL SECTION

General information: Pyridine (**B**), carboxylic acids (**C1**-**C10**), and solvents used for syntheses, NMR and ITC experiments, and crystallizations were purchased from Sigma Aldrich or Oakwood Chemicals (Estill SC, USA). The C_{ethyl}-2-methylresorcinarene (**A**) was synthesized according to reported procedures.[68] The ^{1}H, ^{19}F -NMR, DOSY and NOESY NMR experiments were carried out in CD_3OD at 298 K on a either Bruker Avance 300, 400 or 500 MHz spectrometers. **ITC** measurements were performed using VP-ITC instrument made by MicroCal.

Solid-state X-ray crystallography: Data for **B·C1** was measured on a Bruker-Nonius Kappa CCD diffractometer equipped with an APEX-II CCD detector using graphite-monochromated Mo-Kα (λ = 0.71073 Å) radiation.[69] The data for **A·B·C5** were collected using a Rigaku SuperNova single-source Oxford diffractometer with an Atlas EoS CCD detector using mirror-monochromated Mo-Kα (λ = 0.71073 Å) radiation. Single-crystal X-ray data for **A·B**, **A·C6**, **A·B·C1**, **A·B·C7**, **A·B·C9**, and **A·B·C10**·was measured using a Rigaku SuperNova dual-source Oxford diffractometer equipped with an Atlas detector using mirror-monochromated Cu-Kα (λ = 1.54184 Å) radiation.[70]

Powder X-ray diffraction: The bulk crystallizations were examined by powder X-ray diffraction using a PANalytical X'Pert PRO diffractometer with Cu $K_{\alpha 1}$ radiation (1.5406 Å; 45 kV, 40 mA).

Computational studies: All binary and ternary complexes were optimized using the Gaussian 09 suite of programs[71] at the ωB97X-D/6-311G** level of theory[72], with the polarized continuum solvation model (PCM) to account for solvent effects and the default solvent parameters for methanol. All minima were further confirmed by the presence of only real vibrational frequencies and thermochemical quantities were calculated at 298 K. Further structure analysis and visualizations was performed using GaussView v5.0.8.4 as well as Maestro 10.1.[73] The binding energies for all binary and ternary host–guest assemblies were calculated at B3LYP-D3/6–311G**//ωB97X-D/6-311G** level of theory in a MeOH (PCM) solvation model to account for dispersion interactions. We used Grimme's dispersion corrected functional B3LYP-D3[74] together with long-range corrected (LRC) exchange-correlation functional with inclusion of dispersion correction,

ωB97X-D, to accurately predict the binding energy in those multicomponent supramolecular skeletons which depends on the intermolecular and intramolecular distance. We selected this system based on both its virtues for supramolecular modelling, and because it outperformed other competitor models in a preliminary validation scan. This dual dispersion-corrected functional considers dispersion and range separated corrections and competently describes non-covalent interactions originating from dispersion interactions such as multipole−induced multipole, dipole−dipole, dipole−quadrupole, and polarization permanent multipole-induced multipole, that are all involved in stabilizing the ternary complex. The binding energy (ΔE_b) of **A**·**B**·**C** systems (originated from different intermolecular binning forces) was calculated according to either equation 1 or 2:

$$\Delta E_b = E_{\mathbf{A}\cdot\mathbf{B}\cdot\mathbf{C}} - (E_{\mathbf{B}\cdot\mathbf{C}} + E_{\mathbf{A}}) \quad (1)$$

$$\Delta E_b = E_{\mathbf{A}\cdot\mathbf{B}\cdot\mathbf{C}} - (E_{\mathbf{A}\cdot\mathbf{B}} + E_{\mathbf{C}}) \quad (2)$$

where $E_{(\mathbf{A}\cdot\mathbf{B}\cdot\mathbf{C})}$, $E_{(\mathbf{A}\cdot\mathbf{B})}$, $E_{(\mathbf{B}\cdot\mathbf{C})}$, $E_{(\mathbf{A})}$ and $E_{(\mathbf{A})}$ are the energies of the ternary complex, the binary **B**·**C**, and A·B complexes, as well as **A** and **C** fragments, respectively.

NMR solution experiments: ^{1}H and ^{19}F NMR spectra were recorded on a Bruker Avance 300 MHz (for ^{1}H) and 500 MHz (for ^{19}F) spectrometers. All signals are given as δ values in ppm relative to TMS using residual solvent signals as the internal standard. For sample preparation, stock solutions of the receptor **A** (60 mM), the pyridine, **B** (60 mM), and all the carboxylic acids **Cn** (**n** = **1**-**10**; 60 mM) were prepared in CD_3OD. For the pure **A**, 200 µL of the stock solution was transferred to an NMR tube and diluted with 400 µL of pure CD_3OD providing a 20 mM sample concentration. For the pure **B**, 200 µL of the stock solution was measured into an NMR tube and diluted with 400 µL of pure CD_3OD to give a 20 mM sample concentration. For each of pure carboxylic acids **Cn** (**n** = **1**-**10**), 200 µL of the stock solution was transferred into an NMR tube and diluted with 400 µL of pure CD_3OD to give a 20 mM sample concentration.

For a 1:1 (**A**·**B**) mixture, 200 µL of **A**, 200 µL of **B** and 200 µL of pure CD_3OD provided a 20 mM sample concentration of the each component in the mixture.

For a 1:1 (**A**·**Cn**) mixture, 200 µL of **A**, 200 µL of each **Cn** (**n** = **1**-**10**) and 200 µL of pure CD_3OD provided a 20 mM sample concentration of each component in the mixture.

For a 1:1 (**B**·**Cn**) mixture, 200 µL of **Py**, 200 µL of each **Cn** (**n** = **1**-**10**) and 200 µL of pure CD_3OD provided a 20 mM sample concentration of each component in the mixture.

For a 1:1:1 (**A**·**B**·**Cn**) mixture, 200 µL of **A**, 200 µL of **B** and 200 µL of each **Cn** (n = **1**-**10**) were mixed to give a 20 mM sample concentration of each component in the mixture.

Synthesis of co-crystals: In general, single crystals of binary and ternary complexes were grown by slow evaporation of the respective methanol solutions at room temperature. The prescription of quantities is given below.

*Synthesis of **A**·**B***. To host **A** (21.0 mg, 0.032 mmol) dissolved in methanol (1.0 mL), added pyridine **B** (2.53 mg 0.032 mmol) at room temperature.

*Synthesis of **B**·**C1***. To host **B** (25.0 mg, 0.32 mmol) in methanol (1.0 mL), added trifluoroacetic acid **C1** (36.1 mg 0.032 mmol) at room temperature.

*Synthesis of **A**·**C6***. To host **A** (16.0 mg, 0.024 mmol) in methanol (1.0 mL), added benzoic acid **C6** (2.97 mg 0.024 mmol) at room temperature.

*Synthesis of **A**·**B**·**C1***. To C_{ethyl}-2-methylresorcinarene (**A**) (17.0 mg 0.026 mmol) dissolved in methanol (1.0 mL) sequentially added pyridine **B** (2.10 mg 0.026 mmol) and trifluoroacetic acid **C1** (2.96 mg 0.026 mmol).

*Synthesis of **A**·**B**·**C5***. To C_{ethyl}-2-methylresorcinarene (**A**) (21.0 mg 0.032 mmol) dissolved in methanol (1.0 mL) sequentially added pyridine **B** (2.53 mg 0.032 mmol) and acetic acid **C5** (1.92 mg 0.032 mmol).

*Synthesis of **A**·**B**·**C7***. To C_{ethyl}-2-methylresorcinarene (**A**) (21.5 mg 0.033 mmol) dissolved in methanol (1.0 mL) sequentially added pyridine **B** (2.59 mg 0.033 mmol) and cyclopropane carboxylic acid **C7** (2.84 mg 0.33 mmol).

*Synthesis of **A**·**B**·**C9***. To C_{ethyl}-2-methylresorcinarene (**A**) (20.0 mg 0.031 mmol) dissolved in methanol (1.0 mL) sequentially added pyridine **B** (2.41 mg 0.031 mmol) and cyclopentane carboxylic acid **C9** (3.53 mg 0.032 mmol).

*Synthesis of **A**·**B**·**C10***. To C_{ethyl}-2-methylresorcinarene (**A**) (19.0 mg 0.029 mmol) dissolved in methanol (1.0 mL) sequentially added pyridine **B** (2.29 mg 0.029 mmol) and cyclohexane carboxylic acid **C10** (3.72 mg 0.029 mmol).

ASSOCIATED CONTENT

Supporting Information

The Supporting Information is available free of charge on the ACS Publications website at DOI: xxxx.

Experimental details, copies of the ^{1}H, ^{19}F NMR, DOSY and NOESY data, ITC data, and computational data (PDF).

X-ray crystallographic data for **A**·**B**, **A**·**C6**, **B**·**C1**, **A**·**B**·**C1**, **A**·**B**·**C5, A**·**B**·**C7**, **A**·**B**·**C9**, **and A**·**B**·**C10** can be obtained free of charge from the Cambridge Crystallographic Data Centre via www.ccdc.cam.ac.uk/data_request/cif. CCDC 1938866-1938873 (CIF).

AUTHOR INFORMATION

Corresponding Authors

*Email: kari.t.rissanen@jyu.fi
*Email: rakesh.t.puttreddy@jyu.fi
*Email: j.trant@uwindsor.ca
*Email: beyeh@oakland.edu

ORCID

S. Maryamdokht Taimoory: 0000-0002-5350-227X
Kwaku Twum: 0000-0001-5390-0609
Mohadeseh Dashti: 0000-0001-8200-1602
Fangfang Pan: 0000-0002-3091-6795
Manu Lahtinen: 0000-0001-5561-3259
Kari Rissanen: 0000-0002-7282-8419

Rakesh Puttreddy: 0000-0002-2221-526X
John F. Trant: 0000-0002-4780-4968
Ngong Kodiah Beyeh: 0000-0003-3935-1812

Author Contributions

The manuscript was written and edited through the contributions of all authors. All authors have given approval to the final version of the manuscript. Rakesh Puttreddy: original concept and SCXRD analyses. S. Maryamdokht Taimoory: Computational and NMR analyses. Kwaku Twum: NMR and ITC analyses. Mohadeseh Dashti: NMR analysis. Fangfang Pan: SCXRD analysis, Manu Lahtinen: PXRD analysis. Kari Rissanen: supervised the work in Finland. John F. Trant: supervised the work in Canada. Ngong Kodiah Beyeh: supervised the work in the USA.

Notes

The authors declare no competing financial interest.

ACKNOWLEDGMENTS

The authors gratefully acknowledge financial support from the Academy of Finland (RP: grant# 298817), the University of Jyväskylä, Natural Sciences and Engineering Research Council of Canada (JFT: grant # 2018-06338), National Natural Science Foundation of China (FP: grant# 21602071) and Oakland University, MI, USA. This work was made possible by the facilities of the Shared Hierarchical Academic Research Compu-ting Network (SHARCNET: www.sharcnet.ca) and Compute/Calcul Canada.

REFERENCES

(1) Hunter, C. A.; Anderson, H. L. What Is Cooperativity? *Angew. Chemie Int. Ed.* **2009**, *48*, 7488–7499. https://doi.org/10.1002/anie.200902490.

(2) von Krbek, L. K. S.; Schalley, C. A.; Thordarson, P. Assessing Cooperativity in Supramolecular Systems. *Chem. Soc. Rev.* **2017**, *46*, 2622–2637. https://doi.org/10.1039/C7CS00063D

(3) Mahadevi, A. S.; Sastry, G. N. Cooperativity in Noncovalent Interactions. *Chem. Rev.* **2016**, *116*, 2775–2825. https://doi.org/10.1021/cr500344e.

(4) J Atwood, J. L.; Gokel, G. W.; Barbour, L. *Comprehensive Supramolecular Chemistry II*; Elsevier Science, 2017.

(5) Steed, J. W. The Role of Co-Crystals in Pharmaceutical Design. *Trends Pharmacol. Sci.* **2013**, *34*, 185–193. https://doi.org/https://doi.org/10.1016/j.tips.2012.12.003.

(6) Schultheiss, N.; Newman, A. Pharmaceutical Cocrystals and Their Physicochemical Properties. *Cryst. Growth Des.* **2009**, *9*, 2950–2967. https://doi.org/10.1021/cg900129f.

(7) Shan, N.; Zaworotko, M. J. The Role of Cocrystals in Pharmaceutical Science. *Drug Discov. Today* **2008**, *13*, 440–446. https://doi.org/https://doi.org/10.1016/j.drudis.2008.03.004.

(8) Duggirala, N. K.; Perry, M. L.; Almarsson, Ö.; Zaworotko, M. J. Pharmaceutical Cocrystals: Along the Path to Improved Medicines. *Chem. Commun.* **2016**, *52*, 640–655. https://doi.org/10.1039/C5CC08216A.

(9) Almarsson, Ö.; Peterson, M. L.; Zaworotko, M. The A to Z of Pharmaceutical Cocrystals: A Decade of Fast-Moving New Science and Patents. *Pharm. Pat. Anal.* **2012**, *1*, 313–327. https://doi.org/10.4155/ppa.12.29.

(10) Landenberger, K. B.; Matzger, A. J. Cocrystals of 1,3,5,7-Tetranitro-1,3,5,7-Tetrazacyclooctane (HMX). *Cryst. Growth Des.* **2012**, *12*, 3603–3609. https://doi.org/10.1021/cg3004245.

(11) Landenberger, K. B.; Matzger, A. J. Cocrystal Engineering of a Prototype Energetic Material: Supramolecular Chemistry of 2,4,6-Trinitrotoluene. *Cryst. Growth Des.* **2010**, *10*, 5341–5347. https://doi.org/10.1021/cg101300n.

(12) Bolton, O.; Matzger, A. J. Improved Stability and Smart-Material Functionality Realized in an Energetic Cocrystal. *Angew. Chemie Int. Ed.* **2011**, *50*, 8960–8963. https://doi.org/10.1002/anie.201104164.

(13) Bolton, O.; Simke, L. R.; Pagoria, P. F.; Matzger, A. J. High Power Explosive with Good Sensitivity: A 2:1 Cocrystal of CL-20:HMX. *Cryst. Growth Des.* **2012**, *12*, 4311–4314. https://doi.org/10.1021/cg3010882.

(14) Guo, D.; An, Q.; Zybin, S. V; Goddard III, W. A.; Huang, F.; Tang, B. The Co-Crystal of TNT/CL-20 Leads to Decreased Sensitivity toward Thermal Decomposition from First Principles Based Reactive Molecular Dynamics. *J. Mater. Chem. A* **2015**, *3*, 5409–5419. https://doi.org/10.1039/C4TA06858K.

(15) Park, L. Y.; Hamilton, D. G.; McGehee, E. A.; McMenimen, K. A. Complementary C3-Symmetric Donor−Acceptor Components: Cocrystal Structure and Control of Mesophase Stability. *J. Am. Chem. Soc.* **2003**, *125*, 10586–10590. https://doi.org/10.1021/ja036540o.

(16) Attias, A.-J.; Cavalli, C.; Donnio, B.; Guillon, D.; Hapiot, P.; Malthête, J. Columnar Mesophase from a New Disclike Mesogen Based on a 3,5-Dicyano-2,4,6-Tristyrylpyridine Core. *Chem. Mater.* **2002**, *14*, 375–384. https://doi.org/10.1021/cm010725h.

(17) Bisson, A. P.; Hunter, C. A.; Morales, J. C.; Young, K. Cooperative Interactions in a Ternary Mixture. *Chem. – A Eur. J.* **1998**, *4*, 845–851. https://doi.org/10.1002/(SICI)1521-3765(19980515)4:5<845::AID-CHEM845>3.0.CO;2-%23.

(18) Topić, F.; Rissanen, K. Systematic Construction of Ternary Cocrystals by Orthogonal and Robust Hydrogen and Halogen Bonds. *J. Am. Chem. Soc.* **2016**, *138*, 6610–6616. https://doi.org/10.1021/jacs.6b02854.

(19) Tothadi, S.; Desiraju, G. R. Designing Ternary Cocrystals with Hydrogen Bonds and Halogen Bonds. *Chem. Commun.* **2013**, *49*, 7791–7793. https://doi.org/10.1039/C3CC43822H.

(20) Aakeröy, C. B.; Desper, J.; Smith, M. M. Constructing, Deconstructing, and Reconstructing Ternary Supermolecules. *Chem. Commun.* **2007**, 38, 3936–3938. https://doi.org/10.1039/B707518A.

(21) Tothadi, S.; Mukherjee, A.; Desiraju, G. R. Shape and Size Mimicry in the Design of Ternary Molecular Solids: Towards a Robust Strategy for Crystal Engineering. *Chem. Commun.* **2011**, *47*, 12080–12082. https://doi.org/10.1039/C1CC14567C.

(22) Rest, C.; Kandanelli, R.; Fernández, G. Strategies to Create Hierarchical Self-Assembled Structures via Cooperative Non-Covalent Interactions. *Chem. Soc. Rev.* **2015**, *44*, 2543–2572. https://doi.org/10.1039/C4CS00497C.

(23) Botta, B.; Cassani, M.; D'Acquarica, I.; Subissati, D.; Monache, G.

Z. and G. D. Resorcarenes: Hollow Building Blocks for the Host-Guest Chemistry. *Current Organic Chemistry*. 2005, pp 1167–1202. https://doi.org/http://dx.doi.org/10.2174/1385272054553613.

(24) Sliwa, W.; Kozlowski, C. *Calixarenes and Resorcinarenes*; Wiley, 2009.

(25) Schneider, H.-J.; Schneider, U. The Host-Guest Chemistry of Resorcinarenes. *J. Incl. Phenom. Mol. Recognit. Chem.* **1994**, *19*, 67–83. https://doi.org/10.1007/BF00708975.

(26) McIldowie, M. J.; Mocerino, M.; Ogden, M. I. A Brief Review of C n -Symmetric Calixarenes and Resorcinarenes. *Supramol. Chem.* **2010**, *22*, 13–39. https://doi.org/10.1080/10610270902980663.

(27) Rebek. Jr. J. Molecular Behavior in Small Spaces. *Acc. Chem. Res.* **2009**, *42*, 1660–1668. https://doi.org/10.1021/ar9001203.

(28) Shivanyuk. A. Selective formation of heterodimeric resorcinarene capsules *Tetrahedron* **2005**, *61*, 349–352. https://doi.org/10.1016/j.tet.2004.10.089.

(29) Evan-Salem, T.; Baruch, I.; Avram, L.; Cohen, Y.; Palmer, L. C.; Rebek. J. Resorcinarenes are hexameric capsules in solution. *Proc. Natl. Acad. Sci.* **2006**, *103*, 12296–12300. https://doi.org/10.1073/pnas.0604757103.

(30) Adriaenssens, L.; Ballester. P. Hydrogen bonded supramolecular capsules with functionalized interiors: the controlled orientation of included guests. *Chem. Soc. Rev.* **2013**, *42*, 3261–3277. https://doi.org/10.1039/C2CS35461F.

(31) Rauwald, U.; Scherman. O. A.; Supramolecular Block Copolymers with Cucurbit[8]uril in Water. *Angew. Chemie Int. Ed.* **2008**, *47*, 3950–3953. https://doi.org/10.1002/anie.200705591.

(32) Al'tshuler, G. N.; Fedyaeva, O. N.; Ostapova. E. V. The reaction ofC-phenylcalix[4]resorcinarene-based polymer with quaternary ammonium and potassium cations. *Russ. Chem. Bull.* **2000**, *49*, 1468–1470. https://doi.org/10.1007/BF02495099.

(33) Fujimura, T.; Ramasamy, E.; Ishida, Y.; Shimada, T.; Takagi, S.; Ramamurthy. V. Sequential energy and electron transfer in a three-component system aligned on a clay nanosheet. *Phys. Chem. Chem. Phys.* **2016**, *18*, 5404–5411. https://doi.org/10.1039/C5CP06984J.

(34) Yusof, N. N. M.; Kikuchi, Y.; Kobayashi, T. Predominant hosting lead(II) in ternary mixtures of heavy metal ions by a novel of diethylaminomethyl-calix[4]resorcinarene. *Int. J. Environ. Sci. Technol.* **2014**, *11*, 1063–1072. https://doi.org/10.1007/s13762-013-0298-9.

(35) Beyeh, N. K.; Pan, F.; Rissanen. K. Hierarchical Ordering in Ternary Co-Crystals of C_{60}, *N*-Benzyl Ammonium Resorcinarene Bromide and Solvent Molecules. *Cryst. Growth Des.* **2014**, *14*, 6161–6165. https://doi.org/10.1021/cg5014413.

(36) Appel, E. A.; Biedermann, F.; Rauwald, U.; Jones, S. T.; Zayed, J. M.; Scherman. O. A. Supramolecular Cross-Linked Networks *via* Host–Guest Complexation with Cucurbit[8]uril. *J. Am. Chem. Soc.* **2010**, *132*, 14251–14260. https://doi.org/10.1021/ja106362w.

(37) Rauwald, U.; Biedermann, F.; Deroo, S.; Robinson, C. V.; Scherman. O. A. Correlating Solution Binding and ESI-MS Stabilities by Incorporating Solvation Effects in a Confined Cucurbit[8]uril System. *J. Phys. Chem. B* **2010**, *114*, 8606–8615. https://doi.org/10.1021/jp102933h.

(38) Sindelar, V.; Cejas, M. A.; Raymo, F. M.; Chen, W.; Parker, S. E.; Kaifer. A. E. Supramolecular Assembly of 2,7-Dimethyldiazapyrenium and Cucurbit[8]uril: A New Fluorescent Host for Detection of Catechol and Dopamine. *Chem. – A Eur. J.* **2005**, *11*, 7054–7059. https://doi.org/10.1002/chem.200500917.

(39) Nguyen, N.; Clements, A. R.; Pattabiraman. M. Using non-covalent interactions to direct regioselective 2+2 photocycloaddition within a macrocyclic cavitands. *New J. Chem.* **2016**, *40*, 2433–2443. https://doi.org/10.1039/C5NJ02376A.

(40) Kumar, M.; Kumaraswamy. G. Phase behaviour of the ternary system: monoolein–water–branched polyethylenimine. *Soft Matter* **2015**, *11*, 5705–5711. https://doi.org/10.1039/C5SM01082A.

(41) Basílio, N.; Francisco, V.; García-Río. L. Independent Pathway Formation of Guest–Host in Host Ternary Complexes Made of Ammonium Salt, Calixarene, and Cyclodextrin. *J. Org. Chem.* **2012**, *77*, 10764–10772. https://doi.org/10.1021/jo302074x.

(42) Wang, Z.; Liu, K.; Wang, P.; Xu, D.; Gao, J.; Zhang, L.; Li, M.; Wang. Y. Liquid–Liquid Equilibrium Measurements and Correlation for Ternary Systems (Butyl Acetate + 1-Butanol + Ethylene Glycol/1,3-Propanediol/Ethanolamine) at 298.15 K. *J. Chem. Eng. Data* **2019**, *64*, 3244–3249. https://doi.org/10.1021/acs.jced.8b01219.

(43) Ma, X.; Zhao. Y. Biomedical Applications of Supramolecular Systems Based on Host–Guest Interactions. *Chem. Rev.* **2015**, *115*, 7794–7839. https://doi.org/10.1021/cr500392w.

(44) Mahadevan, K.; Patthipati, V. S.; Han, S.; Swanson, R. J.; Whelan, E. C.; Osgood, C.; Balasubramanian. R. Highly fluorescent resorcinarene cavitand nanocapsules with efficient renal clearance. *Nanotechnology*, **2016**, *27*, 335101. https://doi.org/10.1088/0957-4484/27/33/335101.

(45) Davis, M. M.; Boyd. S. D. Recent progress in the analysis of αβT cell and B cell receptor repertoires. *Curr. Opin. Immunol.* **2019**, *59*, 109–114. DOI: 10.1016/j.coi.2019.05.012

(46) Tsai, S.; Santamaria. P. MHC class II polymorphisms, autoreactive T-cells, and autoimmunity. *Front. Immunol.* **2013**, *4*, 321. https://doi.org/10.3389/fimmu.2013.00321.

(47) Meister, D. Taimoory, S. M.; Trant. J. F. Unnatural amino acids improve affinity and modulate immunogenicity: Developing peptides to treat MHC type II autoimmune disorders. *Pept. Sci.* **2019**, *111*, e24058. https://doi.org/10.1002/pep2.24058.

(48) Kim, C.-Y.; Quarsten, H.; Bergseng, E.; Khosla, C.; Sollid. L. M. Structural basis for HLA-DQ2-mediated presentation of gluten epitopes in celiac disease. *Proc. Natl. Acad. Sci.* **2004**, *101*, 4175–4179. https://doi.org/10.1073/pnas.0306885101.

(49) Puttreddy, R.; Beyeh, N. K.; Rissanen, K. Inclusion Complexes of C_{ethyl}-2-Methylresorcinarene and Pyridine N-Oxides: Breaking the C-I···O-N^+ Halogen Bond by Host-Guest Complexation. *CrystEngComm* **2016**, *18*, 793–799. https://doi.org/10.1039/c5ce02354h.

(50) Puttreddy, R.; Beyeh, N. K.; Ras, R. H. A.; Trant, J. F.; Rissanen, K. Endo-/Exo- and Halogen-Bonded Complexes of Conformationally Rigid C_{ethyl}-2-Bromoresorcinarene and Aromatic N-Oxides. *CrystEngComm* **2017**, *19* (30), 4312–4320. https://doi.org/10.1039/C7CE00975E.

(51) Puttreddy, R.; Beyeh, N. K.; Kalenius, E.; Ras, R. H. A.; Rissanen, K. 2-Methylresorcinarene: A Very High Packing Coefficient in a Mono-Anion Based Dimeric Capsule and the X-Ray Crystal Structure of the Tetra-Anion. *Chem. Commun.* **2016**, *52*, 8115–8118. https://doi.org/10.1039/c6cc03289c.

(52) Beyeh, N. K.; Puttreddy, R. Methylresorcinarene: A Reaction Vessel to Control the Coordination Geometry of Copper(II) in Pyridine N-Oxide Copper(II) Complexes. *Dalt. Trans.* **2015**, *44*, 9881–9886. https://doi.org/10.1039/C5DT01143D.

(53) Beer, P. D.; Gale, P. A. Anion Recognition and Sensing: The State of the Art and Future Perspectives. *Angew. Chemie Int. Ed.* **2001**, *40*, 486–516. **https://doi.org/10.1002/1521-3773(20010202)40:3<486::AID-ANIE486>3.0.CO;2-P**.

(54) Roelens, S.; Vacca, A.; Venturi, C. Binding of Ionic Species: A General Approach To Measuring Binding Constants and Assessing Affinities. *Chem. – A Eur. J.* **2009**, *15*, 2635–2644. **https://doi.org/10.1002/chem.200802298**.

(55) Beyeh, N. K.; Göth, M.; Kaufmann, L.; Schalley, C. A.; Rissanen, K. The Synergetic Interplay of Weak Interactions in the Ion - Pair Recognition of Quaternary and Diquaternary Ammonium Salts by Halogenated Resorcinarenes. *Eur. J. Org. Chem.* **2014**, 80–85. **https://doi.org/10.1002/ejoc.201300886**.

(56) Nissinen, M.; Rissanen, K. Crystal Engineering Studies of the Complexes of Ethyl Resorcinarene with Aromatic Nitrogen Heterocycles. *Supramol. Chem.* **2003**, *15*, 581–590. https://doi.org/10.1080/1061027031000160517 9.

(57) Hynes, M. J. EQNMR: a computer program for the calculation of stability constants from nuclear magnetic resonance chemical shift data. *J. Chem. Soc. Dalton Trans.* **1993**, 311 –312. **https://doi.org/10.1039/DT9930000311**.

(58) Cohen, Y.; Avram, L.; Frish, L.. Diffusion NMR Spectroscopy in Supramolecular and Combinatorial Chemistry: An Old Parameter—New Insights. *Angew. Chemie Int. Ed.* **2005**, *44*, 520–554. **https://doi.org/10.1002/anie.200300637**.

(59) Avram, L.; Cohen, Y.; Rebek Jr. J. Recent advances in hydrogen-bonded hexameric encapsulation complexes. *Chem. Commun.* **2011**, *47*, 5368–5375. **https://doi.org/10.1039/C1CC10150A**.

(60) Avram, L.; Cohen. Y. Diffusion NMR of molecular cages and capsules. *Chem. Soc. Rev.* **2015**, *44*, 586–602. **https://doi.org/10.1039/C4CS00197D**.

(61) Avram, L.; Cohen. Y. Spontaneous Formation of Hexameric Resorcinarene Capsule in Chloroform Solution as Detected by Diffusion NMR. *J. Am. Chem. Soc.* **2002**, *124*, 15148–15149. https://doi.org/10.1021/ja0272686.

(62) Kato, H.; Saito, T.; Nabeshima, M.; Shimada, K.; Kinugasa. S. Assessment of diffusion coefficients of general solvents by PFG-NMR: investigation of the sources error. *J. Magn. Reson.* **2006**, *180*, 266–273. DOI: 10.1016/j.jmr.2006.03.003.

(63) Bruno, I. J.; Cole, J. C.; Edgington, P. R.;. Kessler, M.; Macrae, C. F.; McCabe, P.; Pearson, J.; Taylor. R. New software for searching the Cambridge Structural Database and visualizing crystal structures. *Acta Crystallogr. Sect. B* **2002**, *58*, 389–397. https://doi.org/10.1107/S0108768102003324.

(64) Gilli, P.; Pretto, L.; Bertolasi, V.; Gilli. G. Predicting Hydrogen-Bond Strengths from Acid−Base Molecular Properties. The pK_a Slide Rule: Toward the Solution of a Long-Lasting Problem. *Acc. Chem. Res.* **2009**, *42*, 33–44. https://doi.org/10.1021/ar800001k.

(65) Biedermann, F.; Schneider. H.-J. Experimental Binding Energies in Supramolecular Complexes. *Chem. Rev.* **2016**, *116*, 5216–5300. https://doi.org/10.1021/acs.chemrev.5b00583.

(66) Deutman, A. B. C.; Monnereau, C.; Moalin, M.; Coumans, R. G. E.; Veling, N.; Coenen, M.; Smits, J. M. M.; de Gelder, R.; Elemans, J. A. A. W.; Ercolani, G.; Nolte, R. J. M.; Rowan, A. E. Squaring cooperative binding circles. *Proc. Natl. Acad. Sci.* **2009**, *106*, 10471 LP – 10476. https://doi.org/10.1073/pnas.0810145106.

(67) Williamson. J. R. Cooperativity in macromolecular assembly. *Nat. Chem. Biol.* **2008**, *4*, 458. https://doi.org/10.1038/nchembio.102.

(68) Beyeh, N. K.; Weimann, D. P.; Kaufmann, L.; Schalley, C. A. and Rissanen, K. Ion-Pair Recognition of Tetramethylammonium Salts by Halogenated Resorcinarenes. *Chem. – A Eur. J.* **2012**, 18, 5552–5557. **https://doi.org/10.1002/chem.201103991**.

(69) Hooft, R.W.W. COLLECT Data Collection Software, **1998**, Nonius BV, Delft, the Netherlands.

(70) Rigaku Oxford Diffraction, **2017**, *CrysAlisPro* software system, version 38.46, Rigaku Corporation, Oxford, UK.

(71) Frisch, M. J.; Trucks, G. W.; Schlegel, H. B.; Scuseria, G. E.; Robb, M. A.; Cheeseman, J. R.; Scalmani, G.; Barone, V.; Mennucci, B.; Petersson, G. A.; Nakatsuji, H.; Caricato, M.; Li, X.; Hratchian, H. P.; Izmaylov, A. F.; Bloino, J.; Zhang, G.; Sonnenberg, J. L.; Hada, M.; Ehara, M.; Toyota, K.; Fukuda, R.; Hasegawa, J.; Ishida, M.; Nakajima, T.; Honda, Y.; Kitao, O.; Nakai, H.; Vreven, T.; Montgomery, J. A.; Peralta, Jr., J. E.; Ogliaro, F.; Bearpark, M.; Heyd, J. J.; Brothers, E.; Kudin, K. N.; Staroverov, V. N.; Kobayashi, R.; Normand, J.; Raghavachari, K.; Rendell, A.; Burant, J. C.; Iyengar, S. S.; Tomasi, J.; Cossi, M.; Rega, N.; Millam, J. M.; Klene, M.; Knox, J.e.; Cross, J. B.; Bakken, V.; Adamo, C.; Jaramillo, J.; Gomperts, R.; Stratmann, R. E.; Yazyev, O.; Austin, A. J.; Cammi, A. R.; Pomelli, C.; Ochterski, J. W.; Martin, R. L.; Morokuma, K.; Zakrzewski, V. G.; Voth, G. A.; Salvador, P.; Dannenberg, J. J.; Dapprich, S.; Daniels, A. D.; Farkas, Ö.; Foresman, J. B.; Ortiz, J. V.; Cioslowski, J.; Fox, D. J. Gaussian 09, Revision D.02; Gaussian, Inc., Wallingford, CT, **2009**.

(72) Chai, J.-D.; Head-Gordon, M. Long-range corrected hybrid density functionals with damped atom–atom dispersion corrections. *Phys. Chem. Chem. Phys.* **2008**, *10*, 6615–6620. **https://doi.org/10.1039/B810189B**

(73) (a) Schrödinger Release 2017-2: MacroModel, Schrödinger, LLC, New York, NY, **2017**; (b) Schrödinger Release 2017-2: Maestro, Schrödinger, LLC, New York, NY, **2017**.

(74) Grimme, S.; Antony, J.; Ehrlich, S.; Krieg, H. A consistent and accurate ab initio parametrization of density functional dispersion correction (DFT-D) for the 94 elements H-Pu. *J. Chem. Phys.* **2010**, *132*, 154104. DOI: 10.1063/1.3382344

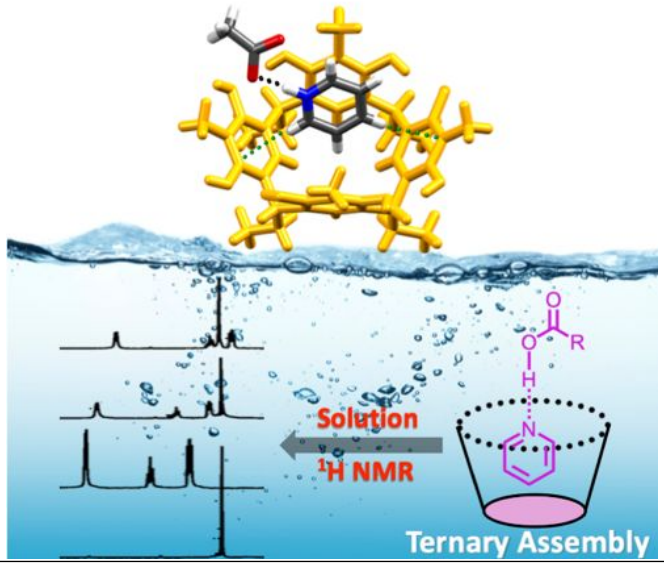
Solution
^{1}H NMR
Ternary Assembly